AGU PUBLICATIONS

JGR

Journal of Geophysical Research: Oceans

RESEARCH ARTICLE

10.1002/2017JC013017

Physical Mechanisms Routing Nutrients in the Central Red Sea

Nikolaos D. Zarokanellos[1], Benjamin Kürten[1], James H. Churchill[2], Cornelia Roder[1,3], Christian R. Voolstra[1], Yasser Abualnaja[1], and Burton H. Jones[1]

[1]Red Sea Research Center (RSRC), Biological and Environmental Sciences & Engineering Division (BESE), King Abdullah University of Science and Technology (KAUST), Thuwal, Saudi Arabia, [2]Department of Physical Oceanography, Woods Hole Oceanographic Institution, Woods Hole, MA, USA, [3]Alfred-Wegener-Institute, Helmholtz Center for Polar and Marine Research, Section of Shelf Sea System Ecology, Helgoland, Germany

Key Points:
- Eastern boundary currents transport episodically patches of less salty and warmer water with higher biomass from the southern toward the CRS
- A cyclonic/anticyclonic eddy pair in spring created an upward nutrient flux and increased the integrated chlorophyll in the oligotrophic CRS
- Higher chlorophyll and CDOM and lower N:P ratios reveal the influence of the eastern boundary current compared with an eddy pair

Supporting Information:
- Supporting Information S1

Correspondence to:
N. Zarokanellos,
nikolaos.zarokanellos@kaust.edu.sa

Citation:
Zarokanellos, N. D., Kürten, B., Churchill, J. H., Roder, C., Voolstra, C. R., Abualnaja, Y., & Jones, B. H. (2017). Physical mechanisms routing nutrients in the central Red Sea. *Journal of Geophysical Research: Oceans*, *122*, 9032–9046. https://doi.org/10.1002/2017JC013017

Received 25 APR 2017
Accepted 28 SEP 2017
Accepted article online 6 OCT 2017
Published online 22 NOV 2017

Abstract Mesoscale eddies and boundary currents play a key role in the upper layer circulation of the Red Sea. This study assesses the physical and biochemical characteristics of an eastern boundary current (EBC) and recurrent eddies in the central Red Sea (CRS) using a combination of in situ and satellite observations. Hydrographic surveys in November 2013 (autumn) and in April 2014 (spring) in the CRS (22.15°N–24.1°N) included a total of 39 and 27 CTD stations, respectively. In addition, high-resolution hydrographic data were acquired in spring 2014 with a towed undulating vehicle (ScanFish). In situ measurements of salinity, temperature, chlorophyll fluorescence, colored dissolved organic matter (CDOM), and dissolved nitrate: phosphorous ratios reveal distinct water mass characteristics for the two periods. An EBC, observed in the upper 150 m of the water column during autumn, transported low-salinity and warm water from the south toward the CRS. Patches of the low-salinity water of southern origin tended to contain relatively high concentrations of chlorophyll and CDOM. The prominent dynamic feature observed in spring was a cyclonic/anticyclonic eddy pair. The cyclonic eddy was responsible for an upward nutrient flux into the euphotic zone. Higher chlorophyll and CDOM concentrations, and concomitant lower nitrate:phosphorous ratios indicate the influence of the EBC in the CRS at the end of the stratified summer period.

1. Introduction

The Red Sea is a geologically young ocean formed by the spreading between the African and Arabian tectonic plates (Rasul et al., 2015). It is primarily forced by thermohaline processes and a monsoonally modulated along basin wind system (Sofianos & Johns, 2002; Yao et al., 2014b). Evaporation, insignificant precipitation and riverine inflow, and a limited connection to the Indian Ocean cause the Red Sea to be one of the saltiest, warmest, and predominantly oligotrophic oceans in the world (Edwards, 1987; Grasshoff, 1969). Modeling and observational studies indicate that the near-surface circulation of the Red Sea is dominated by mesoscale eddies and narrow boundary currents (e.g., Yao et al., 2014a, 2014b; Zhan et al., 2014). The potential impact of such mesoscale features on the Red Sea ecosystem has been highlighted by a number of recent studies.

It has become clear that mesoscale circulation features play an important role in the transport of the water flowing into the Red Sea from the Indian Ocean. This influx into the Red Sea varies seasonally and is evidenced by two intruding water masses with distinct physical and biochemical characteristics. One, Gulf of Aden intermediate water (GAIW), enters the Red Sea as a subsurface layer during summer (Churchill et al., 2014; Johns & Sofianos, 2012; Murray & Johns, 1997; Özgökmen et al., 2003; Yao et al., 2014a, 2014b). The second, Gulf of Aden surface water (GASW), is transported into Red Sea as a surface flow in winter (Sofianos & Johns, 2015). Both water masses enter the Red Sea through the Strait of Bab al Mandab as relatively low-salinity intrusions. GAIW is further distinguished from GASW by higher nutrient and chlorophyll concentrations (Bethoux, 1988; Churchill et al., 2014; Ganssen & Kroon, 1991; Maillard & Soliman, 1986; Sofianos & Johns, 2007) and has been identified as the principal source of water-borne nutrients to the Red Sea (Naqvi et al., 1986; Souvermezoglou et al., 1989). The subsequent northward transport and mixing of GAIW create a latitudinal gradient of productivity and biogeography in the Red Sea (Al-Aidaroos et al., 2017; Halim, 1984; Kürten et al., 2014a; Sofianos & Johns, 2007).

Modeling studies and limited observations have indicated that the northward transport of GAIW and GASW through the Red Sea may largely be underpinned by eastern and western boundary currents (Bower & Farrar, 2015). Simulations of the winter flow field show GASW flowing northward within a western boundary current, which veers eastward and reforms as a northward flowing eastern boundary current (EBC) in the central Red Sea (CRS) (Sofianos, 2003; Yao et al., 2014a; Zhai et al., 2015). Summertime flow simulations show that GAIW is transported northward in an EBC (Yao et al., 2014b), consistent with recent survey measurement that show GAIW contained in an EBC and reaching a latitude of 24°N (Churchill et al, 2014; Wafar et al., 2016b). The survey observations further reveal that GAIW is often carried across the Red Sea axis by the circulation of basin-scale eddies (Wafar et al., 2016a).

The prevalence of mesoscale eddies in the Red Sea has been revealed by recent numerical simulations of physical dynamics (Yao et al., 2014a, 2014b), and by analysis of remotely sensed chlorophyll concentrations (Raitsos et al., 2013) and sea surface height data (Zhan et al., 2014). Eddies appear to be topographically trapped in the Red Sea (Quadfasel & Baudner, 1993) and have a typical duration of approximately 6 weeks (Zhan et al., 2014). A number of recent studies have shown that eddies may significantly impact the Red Sea ecosystem. The modeling results of Chen et al. (2014) indicated that mesoscale eddies play an important role in the transport of heat, salt, and biological and chemical constituents in the Red Sea. Numerical simulations presented by Zhan et al. (2014) indicated that that eddies may considerably impact coastal current variability and cause substantial vertical transport at the coastal boundary due to the interaction with the boundary. The impact of eddies on coral reef communities has been proposed by Robitzch et al. (2015), who infer that eddies may substantially contribute to the dispersal of coral larvae, and by Kürten et al. (2014b), who showed that coral reef biota assimilate macronutrients from the oceanic catchment in the Red Sea. As has been observed in the open ocean (Gaube et al., 2014; McGillicuddy et al., 1998; Rodríguez et al., 2001), eddies may appreciably impact primary productivity of the Red Sea. Survey results presented by Kürten et al. (2016) suggest that vertical motion associated with eddy circulation may inject nutrients into the euphotic zone, and thereby play a significant role in driving the biogeochemistry, biological processes, and trophodynamics of plankton in the Red Sea.

An understanding of the impact of mesoscale circulation features on the Red Sea ecosystem is still far from complete largely due to the dearth of 3-dimensional observations specifically targeting these features. Our study was conducted in the oligotrophic CRS, where boundary currents and recurrent eddies are prevalent (Chen et al., 2014; Raitsos et al., 2013; Sofianos & Johns, 2003; Zhai et al., 2015; Zhan et al., 2014). A motivation was to examine the seasonal variability and vertical exchange of nutrients associated with mesoscale features, and to assess whether eddies in the CRS extend to and influence connected benthic ecosystems (see Wyatt et al., 2012). We also sought to assess the importance of the EBC as one source of nutrients in the CRS. To address our goals, we employed a combination of in situ observations, remotely sensed ocean color data, and sea level anomaly data (SLA) acquired in the CRS during autumn 2013 and spring 2014.

The article is organized as follows. Section 2 describes the data sources and methodology. Section 3 presents the results of the present study in three individual subsections. In the first subsection, we delineate the physical and biochemical characteristics of the water masses that are associated with the EBC and the mesoscale eddies in the CRS during fall and spring, and examine the distribution of the GASW and GAIW in relation to chlorophyll and CDOM. In the second and third subsections, we detail how the EBC observed in autumn 2013 and a cyclonic-anticyclonic eddy pair seen in spring 2014 impacted the biogeochemistry of the CRS. We then summarize our findings in section 4, where we discuss the physical and biogeochemical characteristics of and implications for the central Red Sea.

2. Data Sources and Methodology

2.1. Field Sampling

Sampling was carried out over a large part of the eastern CRS (Figure 1a) in fall (12–20 November 2013) at the end of the stratified summer period and in spring (4–11 April 2014) at the onset of seasonal stratification (Churchill et al., 2014). Vertical profiles of conductivity, temperature, depth (CTD), chlorophyll fluorescence (henceforth chlorophyll), and colored dissolved organic matter (CDOM) were acquired to a depth of 900 m from the R/V *Thuwal* using a CTD/water sampler (Ocean Seven 316 Plus CTD multiparameter probe on a General Oceanics Rosette sampler; for detailed information see http://www.idronaut.it/cms/view/products/multiparameter-ctds/environmental-ctds/ocean-even-316iplusi/s300, Idronaut, S. R. L., Italy). Chlorophyll and

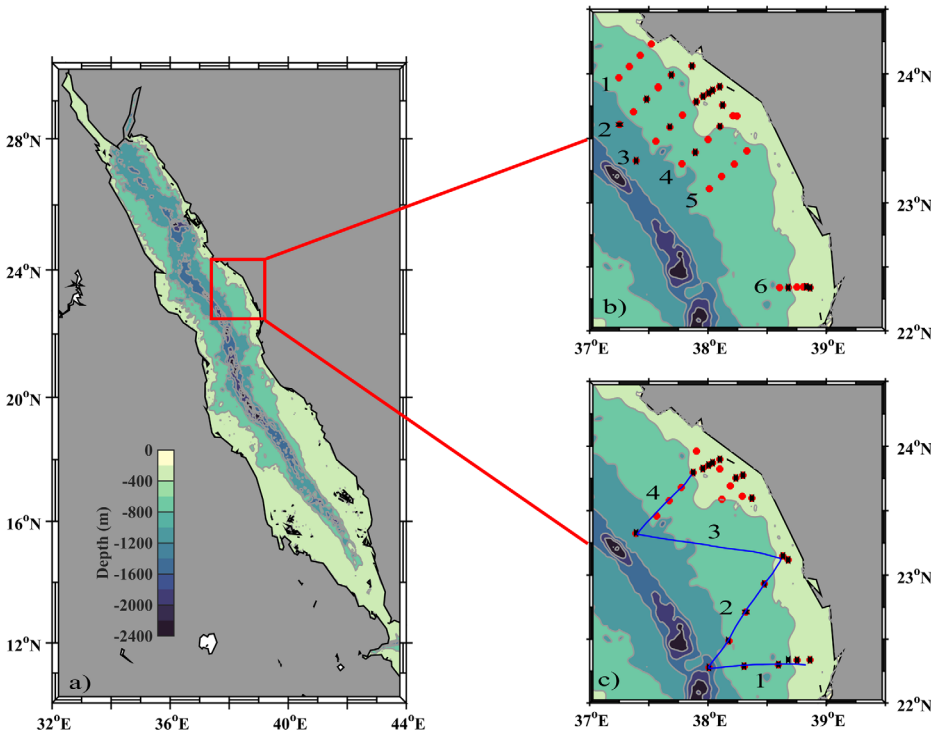

Figure 1. (a) Bathymetric map of the Red Sea. (b) and (c) Smaller-scale maps highlighting ship-based observations carried out in fall (12–20 November 2013) and spring (04–10 April 2014). The red circles mark the locations of CTD casts, and the black crosses indicate the stations where water samples were collected. The blue line traces the ScanFish survey track.

CDOM fluorescence and turbidity were measured with a WETLabs ECO sensor with excitation/emission wavelength pairs of 470/695 nm for chlorophyll, 370/460 nm for CDOM, and backscattering was measured at 700 nm.

Fall surveying was carried out over six east-west transects with 39 hydrographic stations, 17 of which were water-sampling stations (Figure 1b). The April survey covered two east-west transects, 27 hydrographic stations, with 15 water-sampling stations (Figure 1c). Shipboard measurements in April were preceded by a towed vehicle survey (ScanFish II, EIVA) extending from the Shib' Nazar coral reef system (22.29°N) to the inshore reefs off Yanbu (23.78°N). Consistency and integratability of ScanFish and rosette CTD data were checked by lowering the ScanFish to 160 m and comparing the respective ScanFish CTD data with data obtained from a CTD rosette cast at the same station (see supporting information Figure S1). No significant differences in Pot. Temperature and Salinity profiles were observed.

The ScanFish survey was conducted in a zig-zag pattern that formed four across-shore transects (Figure 1c). The ScanFish was equipped with a CTD (SBE 9+, Seabird), a fluorescence sensor (FLBTURB, Wetlabs), and oxygen sensor (SBE 43, Seabird). Data from each ScanFish undulation cycle (2–160 m, and 10 min cycle^{-1}) were averaged into individual vertical profiles. Data were transformed onto a grid with a uniform horizontal and vertical spacing of 2 km and 1 m, respectively. Time-stamps were checked for monotony, and GPS-positions were visually validated and interpolated where necessary.

The data from chlorophyll and CDOM sensors during the two cruises were converted to engineering units using the manufacturer calibrations:

$$[\text{chlorophyll, CDOM}] = \text{scale factor} \times (\text{output} - \text{dark counts}) \tag{1}$$

$$\text{Scale Factor} = \frac{\alpha}{(\text{output}_{\alpha} - \text{dark counts})}, \tag{2}$$

where scale factor (SF) from equation (2) is used in equation (1) for the computation of chlorophyll (μg L^{-1}) and CDOM (ppb), respectively. In equation (2), the known concentration a, is the constituent of chlorophyll

or CDOM, and output$_\alpha$ is the measured signal output for the known concentration. A moving average filter with window size 5 m has been applied in chlorophyll and CDOM to the vertical profiles. Regions with high irradiance such as the Red Sea tend to have lower fluorescence during the day than at night (Behrenfeld et al., 1999; Kinkade et al., 1999). The ScanFish data set was examined for photochemical fluorescence quenching. No significant quenching was detected in this data set.

The Red Sea has one of the largest evaporation rates in the world's oceans with a loss of approximately 2 m yr^{-1} (Sofianos et al., 2002). Salinity is important in regions with high evaporations and potentially destabilizes the mixed layer (Lee et al., 2000). A density-based estimate of MLD accounts for both salinity and temperature effects. Consequently, we used a density difference, $\Delta\sigma_{\theta,}$ relative to the near surface of $<$0.03 kg m^{-3} to define the mixed layer (de Boyer Montégut et al., 2004). For the hydrographic stations, the MLD was calculated using the 1 m binned vertical profiles data for each station.

The relationships between apparent oxygen utilization (AOU) and nitrate were determined by two-way linear regression analysis (Naqvi et al., 1986). From the relationship of salinity, temperature, and oxygen concentration of our ScanFish survey, we determined dissolved nitrite and nitrate (NOx) and the apparent oxygen utilization (see Churchill et al., 2014). Euphotic depth (Z_e) was estimated using the vertical chlorophyll distribution and a model of the between chlorophyll concentration and light attenuation (Morel & Maritorena, 2001). Ship-based and ScanFish measurements of density have been used to estimate geostrophic velocities. The level of no motion for geostrophic velocity estimates was referenced to 500 m for the fall hydrographic sections. Because the ScanFish survey in spring only penetrated to 160 m, the geostrophic velocity calculation was referenced to 155 m. While this is not optimal, it does provide a relative velocity for the water column above this level. During the ScanFish survey, the geostrophic velocity perpendicular to the transect lines and positive velocities have an eastward component.

Water samples were collected for the determination of nitrate and nitrite (NO_x) and phosphorous (PO_4^{3-}) during CTD upcasts from six depths defined by their oceanographic characteristics, i.e., (1) the depths with lowest oxygen concentrations at each station and referred to as oxygen minimum zone (OMZ), (2) the transition from the aphotic to the euphotic zone (≈200 m), (3) from the depth where the density was 1028 kg m^{-3}, (4) from the deep chlorophyll maximum (DCM), (5) from above the DCM, and (6) from the surface mixed layer (SML; 5 m). Dissolved inorganic nutrient concentrations of NOx, and PO_4^{3-} were determined using Flow Injection Analysis (QuikChem 8000, Lachat Instruments; University of California, Santa Barbara,

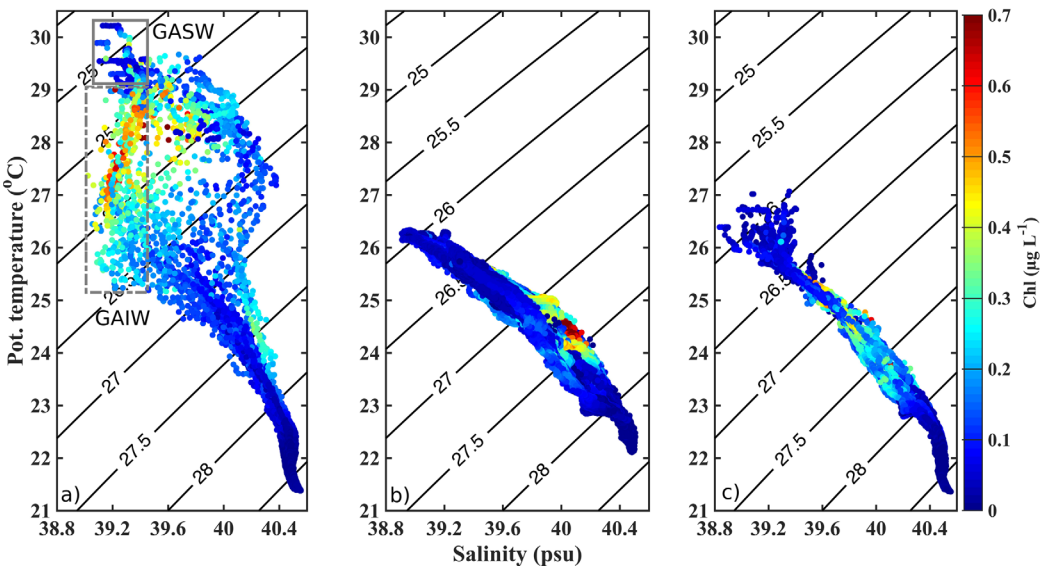

Figure 2. Diagrams of potential temperature-salinity with color indicating chlorophyll (μg L^{-1}) in the central Red Sea: (a) Ship-based observations in November 2013, (b) ScanFish survey in April 2014, and (c) ship-based observations in April 2014. The solid and dash grey box indicate the presence of GASW and GAIW during the November 2013 cruise, respectively.

CA, USA) down to the detection limit of 0.2 for NOx and 0.1 μM for PO_4^{3-}. The remarkable constancy of the Redfield ratio of 16 N:1 P in the global ocean reflects the stabilizing feedback between nitrogen fixation and denitrification (Gruber, 2008). Anomalies of this linear relationship, denoted N* represent the time and space integrated nitrogen deficiency, defined as $N^* = [NO_3–] - 16[PO_4^{3-}] + 2.9$ μmol kg^{-1} (Gruber & Sarmiento, 1997). As N* embodies the combined impact of nitrogen fixation and denitrification N*, one cannot quantitatively distinguish between these two processes. However, the spatial and temporal separation of nitrogen fixation and denitrification allow N* values to be evaluated as a reflection of the overall balance between these two processes (Gruber, 2008).

2.2. Sea Level Anomaly and Ocean Color Chlorophyll Data

SLA data in delayed mode were used to identify and characterize mesoscale eddies and boundary currents in the CRS for both cruise periods. SLA data are based on a multimission altimeter product produced by AVISO and mapped on a regular 0.25° grid (ftp://ftp.aviso.oceanobs.com/global/dt/upd/msla/merged). The merged product combines data from different missions and has fewer mapping errors and better spatial coverage than products created from a single satellite (Ducet et al., 2000). MODIS Level-3 data were obtained from the NASA Ocean Color website (http://oceancolor.gsfc.nasa.gov/).

3. Results

This study investigates two dynamical features that may impact the nutrient availability in the CRS, i.e., the EBC and mesoscale eddies. We describe the water mass characteristic of both physical features and their

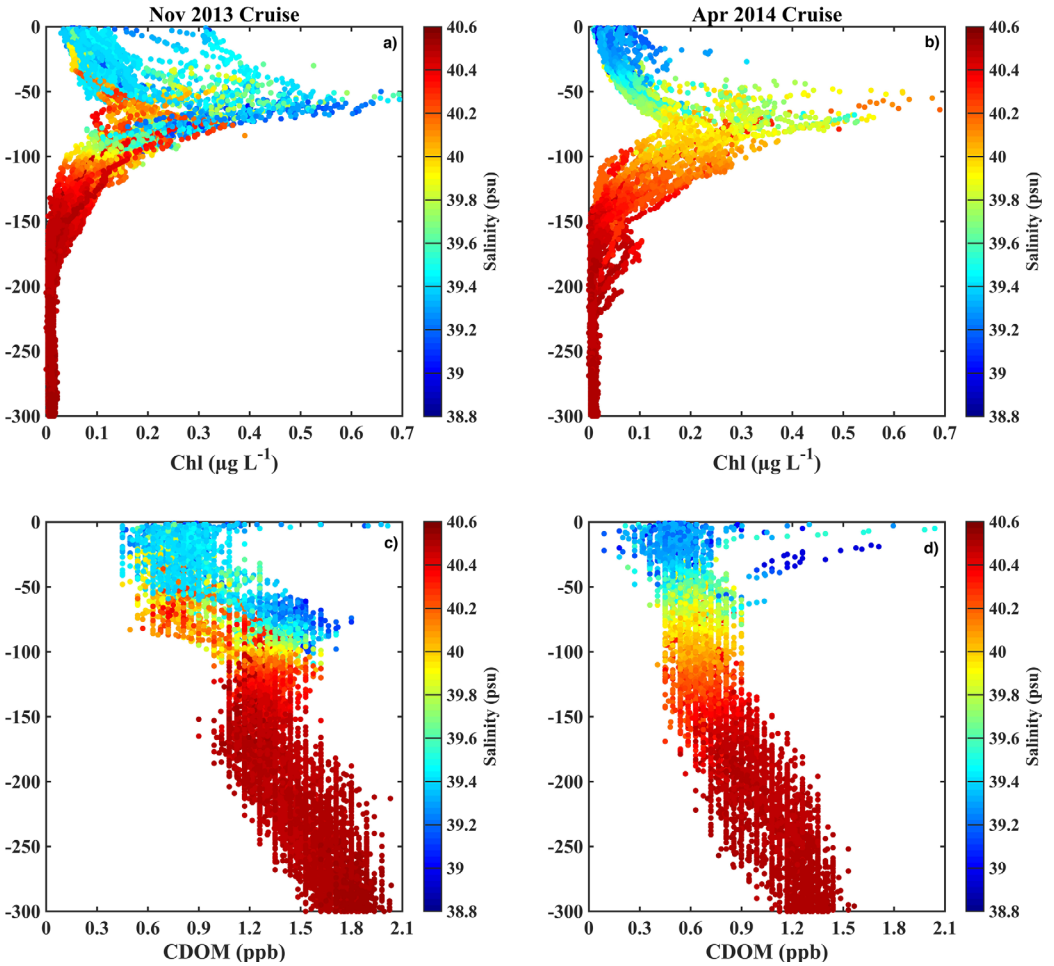

Figure 3. Ship-based vertical profiles of chlorophyll (μg L^{-1}), CDOM concentration (ppb), salinity (color-coded) in (a) and (c) November 2013 and (b) and (d) April 2014.

correlation with biological response parameters that are used as indicators of primary production (i.e., chlorophyll and CDOM).

3.1. Water Masses Characteristics in the Central Red Sea

The theta-S diagrams in Figure 2 show distinct changes in the water mass distribution between the two cruise periods. The November cruise occurs at a time when the inflow to the Red Sea is changing from summer when there is a distinct inflow of Gulf of Aden Intrusion (or Intermediate) Water (GAIW) and the wind forcing is uniformly to the south-southeast along the entire Red Sea to the winter period when there is north-northwest wind in the southern half of the Red Sea and there is an inflow of Gulf of Aden Surface Water into the southern Red Sea. We see the evidence of GAIW in Figure 2a, where lower-salinity water centered between the 26 and 26.5 isopycnal surfaces is indicative of this water advecting into the CRS (Churchill et al., 2014; Sofianos & Johns, 2015). Because this water is subsurface, diapycnal mixing creates a gradient between this intrusion water and the shallower, warmer, high-salinity water in the upper layer. The highest chlorophyll occurs in this gradient region, apparently fueled by the nutrients that were present as the GAIW entered the southern Red Sea and advected northward as shown by Churchill et al. (2014). Warmer (>29 °C) and fresher (<39.4) water is consistent with the influence of Gulf of Aden Surface Water (GASW) advecting into the CRS. According to Yao et al. (2014b) and Sofianos and Johns (2015) surface flow of GASW into the Red Sea begins in September–October when the winds in the southern Red Sea reverse. Thus, by November, it is likely that both GAIW and GASW were present in the CRS and influenced regions water mass characteristics.

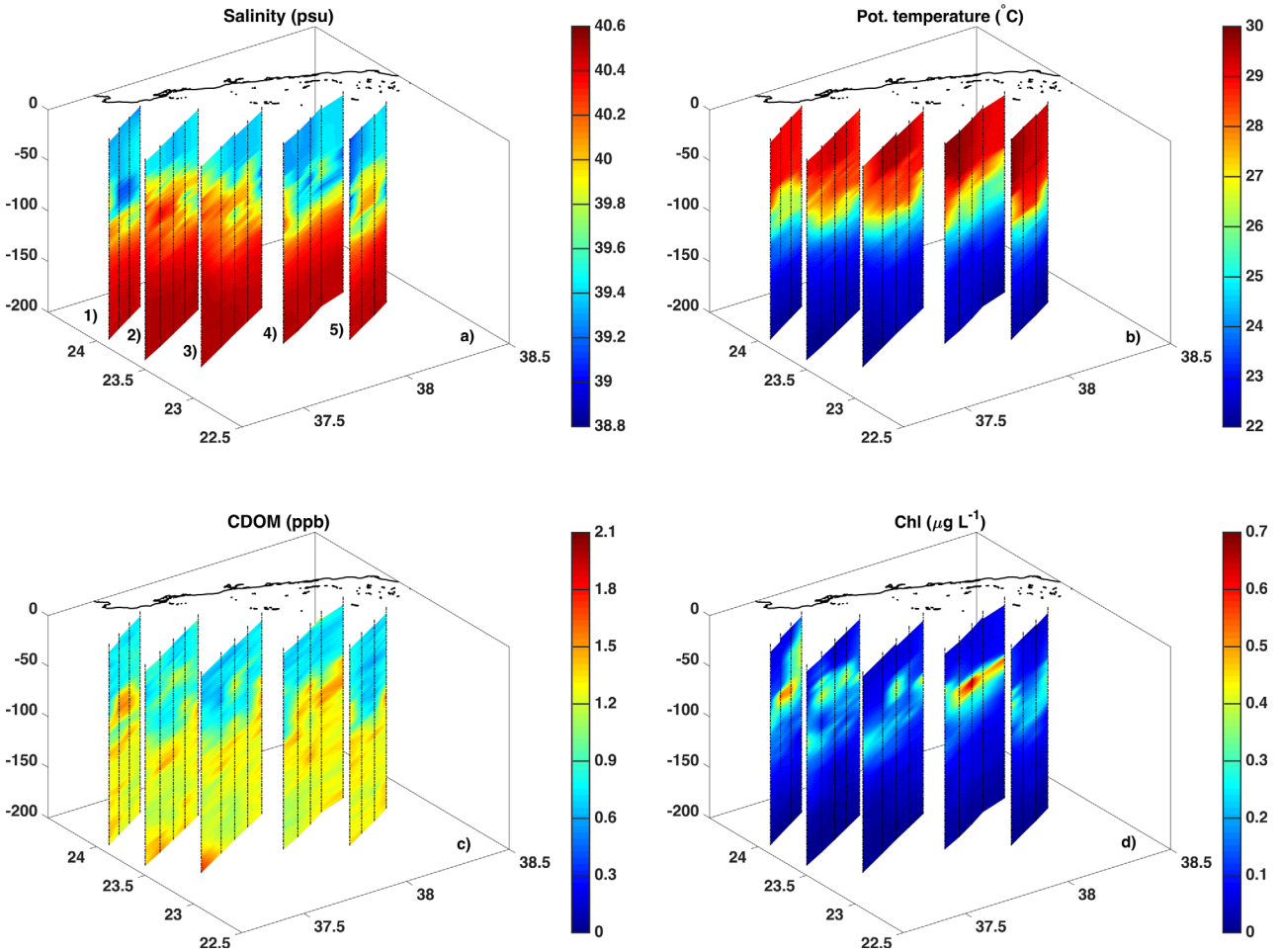

Figure 4. Three-dimensional visualization of (a) salinity, (b) potential temperature (°C), (c) CDOM (ppb), and (d) chlorophyll fluorescence (μg L^{-1}) for the five east-west transects of November 2013.

By April, the theta-S properties have collapsed onto a single mixing line between the intermediate water and the surface water. The combination of continued northward advection of GASW, wintertime vertical mixing, and mixing by eddy activity of the surface water with Red Sea Intermediate Water have resulted in a fairly simple theta-S distribution with the influence of GASW representing the lower salinity endpoint and the higher salinity Red Sea Intermediate Water (Figure 2b). In this case, the higher chlorophyll water is found centered between the 27 and 27.5 isopycnals where the pycnocline interfaces with the euphotic zone. The deeper CTD profiles in Figure 2c show the extension of the interaction between Red Sea Intermediate Water and Red Sea Deep Water.

Vertical profiles of chlorophyll (color-coded for salinity) provide an alternative way to examine the relationship between chlorophyll and CDOM with salinity, indicative of the source water (Figure 3). During fall, the highest chlorophyll concentrations are found between 50 and 75 m and are associated with salinities less than 39.6 (Figure 3a). In spring, the DCM has a similar depth range but salinities associated with the highest chlorophyll concentrations are more than 39.6. There is no significant difference in mean chlorophyll distributions from all ship-based vertical profiles (fall: 0.30 $\pm$0.33 μg L^{-1}, N = 120; spring: 0.25 $\pm$0.28 μg L^{-1}) between the two seasons (two-tailed Mann-Whitney U test, $U = 5010.0$, $n_1 = 90$, $n_2 = 120$, $p < 0.370$), In contrast, the vertical distribution of CDOM is distinctly different between the two seasons (two-tailed Mann-Whitney U test, $U = 2241.0$, $n_1 = 90$, $n_2 = 120$, $p < 0.001$). During the fall, higher CDOM (>1.5 ppb) concentrations are associated with low-salinity at intermediate depths (75–100 m), consistent with the region of GAIW influence. Also in fall, the overall CDOM distribution is 0.3 ppb higher compared with the spring period (Figures 3c and 3d).

3.2. The Physical and Biogeochemical Role of the Eastern Boundary Current

Data from the five east-west transects covered in the fall reveal both the presence of a northward-flowing EBC and large variability of thermohaline and biogeochemical characteristics within the CRS (Figures 4–7).

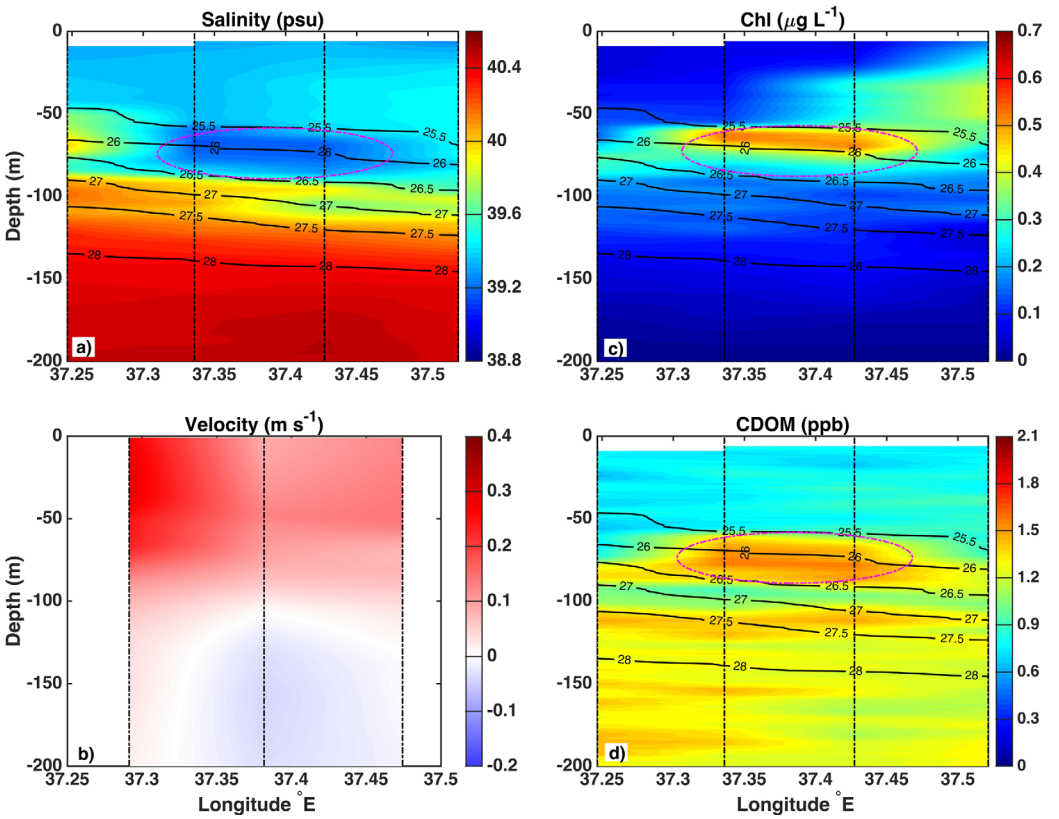

Figure 5. (a) Salinity, (b) geostrophic north-south velocity (reference level of no motion 500 m; positive to the north; m s^{-1}), (c) chlorophyll (μg L^{-1}), and (d) CDOM (ppb) for transect 1 (Figure 1) of November 2013. The dash dot magenta ellipses indicate the location of patches of GAIW.

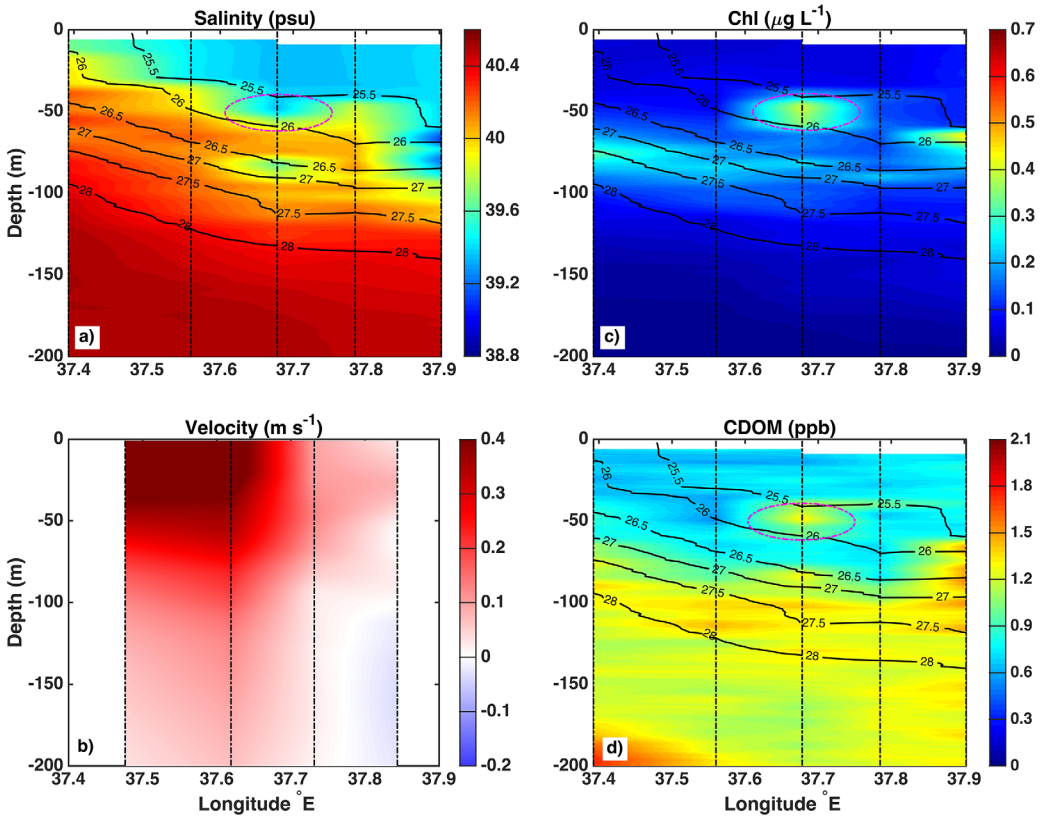

Figure 6. As Figure 5, but for transect 3.

GASW and GAIW are present in the upper layer of the water column as indicated by the vertical distribution of salinity and potential temperature. GASW, with salinities between 39.25 and 39.4, is the dominant water mass in the upper 40–80 m of the water column. Distinct patches of low-salinity GAIW, containing elevated concentrations of CDOM (1.5–1.8 ppb) and chlorophyll (>0.5 μg L^{-1}), appear between σ_Θ of 25.5 to 26.3 and depths of 50 to 75 m, and are apparent as far north as 24.1°N (Figures 4c and 4d). The geostrophic velocities, calculated from the transect data, indicate that these GAIW patches and the GASW water are transported northward by the EBC (Figures 5–7).

The data from the individual transects show considerable variation in the character of the EBC and the water properties associated with it. Along the northernmost transect (transect 1 in Figure 1), a layer of low-salinity water (<39.4) occupies the upper 80 m of the water column and includes both GASW and GAIW (Figure 5a). The EBC, identifiable by isopycnals tilted downward toward the coast, transports these water masses northward at an estimated rate of up to 0.3 m s^{-1} (Figure 5b). GAIW, with salinity lower than 39.25, appears between 37.35 and 37.45°E and between 50 and 75 m depth. Increased chlorophyll and CDOM concentrations are found within the GAIW, which is confined to a σ_Θ range of 25.5–26.3 (Figures 5c and 5d).

The density field of transect 3 shows more upward tilt of the isopycnals offshore perhaps associated with intensification of the EBC (Figures 6a and 6b). The intensified geostrophic currents along this line may be associated with interaction with an offshore eddy (Figure 8a). GASW is the dominant water mass in the upper 50 m. However, a small patch of GAIW is found between 37.6 and 37.75°E as indicated by low-salinity (<39.25), elevated chlorophyll (> 0.3 μg/l), and CDOM concentrations (>1.3 ppb; Figures 6a, 6c, and 6d). The EBC appears further seaward in transect 4 than in the transects to the north as indicated by the distribution of lower salinity water in the upper 50 m and the velocity distribution. GAIW is located between 37.9 and 38.25°E in the 50–70 m depth band and over a σ_Θ range of 25.5–26.3.

Taken together, the transect measurements show that GAIW in the CRS is associated with elevated concentrations of chlorophyll and CDOM and tends to appear in relatively small-scale patches, which during the fall cruise are being transported northward by the EBC (Figures 5−7c and 5−7d). Less salty (<39.4), warmer

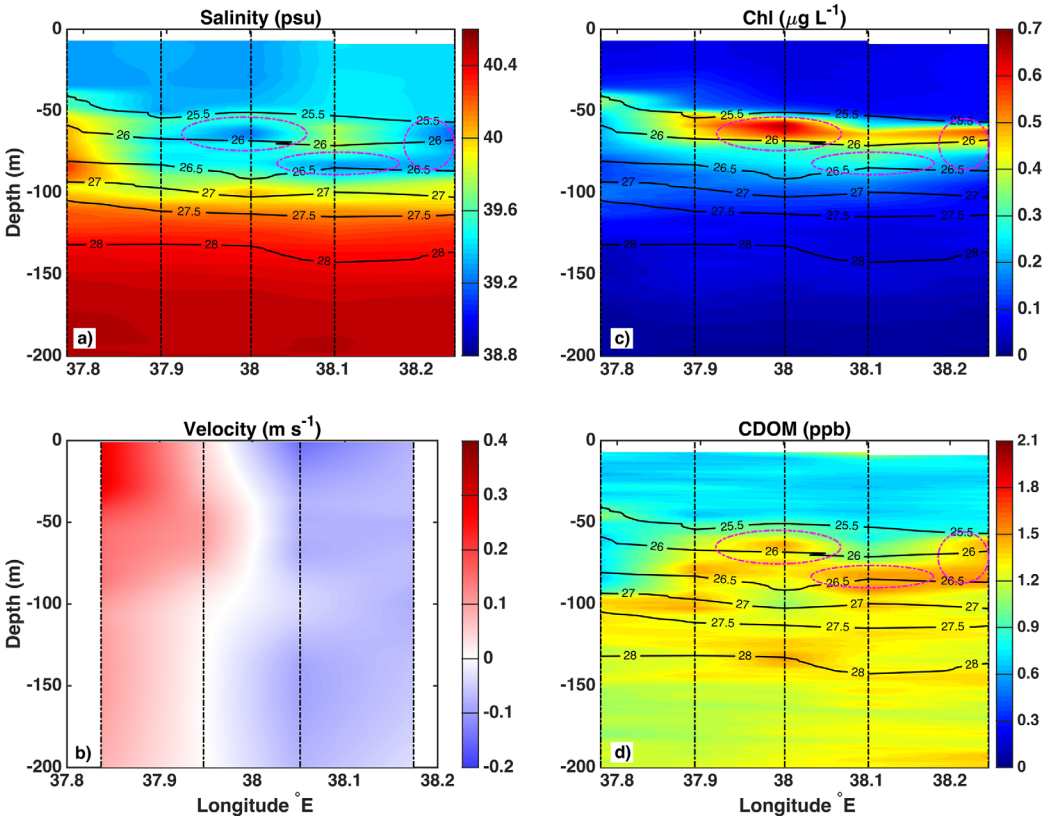

Figure 7. As Figure 5, but for the transect 4.

water (>29°C; temperature section not shown) occupies the first 50 m of the water column between 37.8 and 38.1°E (Figure 7a). A comparison of the salinity and the geostrophic velocities between transects 1, 3, and 4 reveals that the northward flow suggests that EBC is affected by offshore mesoscale eddy activity, as the remote-sensing altimetry indicates in Figure 8a. A similar expansion in width of the EBC and reduction of isopycnal slopes were observed in transect 1 and 4, whereas the EBC is narrower and the isopycnal slopes steeper in transect 3 (Figure 7b).

3.3. The Interactions of Spring-Time Mesoscale Eddies

The ScanFish survey of April 2014 was intended to resolve the eddy features in the CRS that were indicated by the SLA pattern (Figure 8b). The geostrophic velocities resolved from the ScanFish survey are consistent with the SLA pattern with maximum relative velocities of 0.48 m s^{-1} (Figure 9f). Gulf of Aden Surface Water

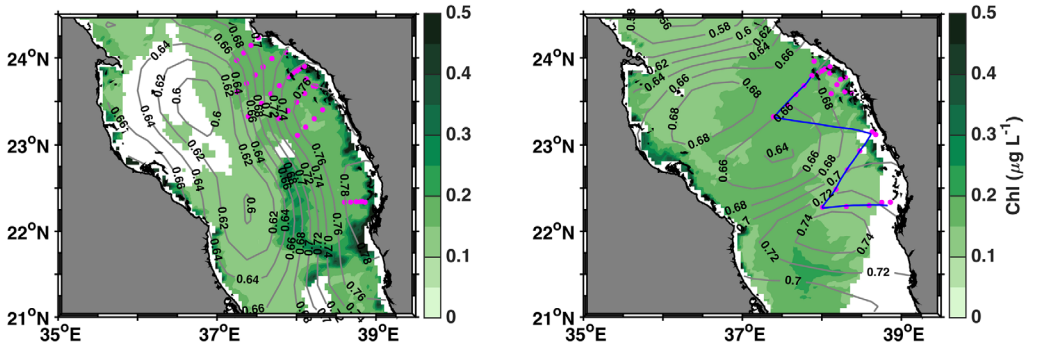

Figure 8. (a) Sea surface chlorophyll distribution (μg L^{-1}) from MODIS Terra satellite on (left) 14 November 2013 and on (right) 14 April 2014. Contour lines represent the mean sea level anomaly (SLA, cm) during the cruise periods. The sampling stations (magenta circles) and the ScanFish survey track (blue line) are shown for reference.

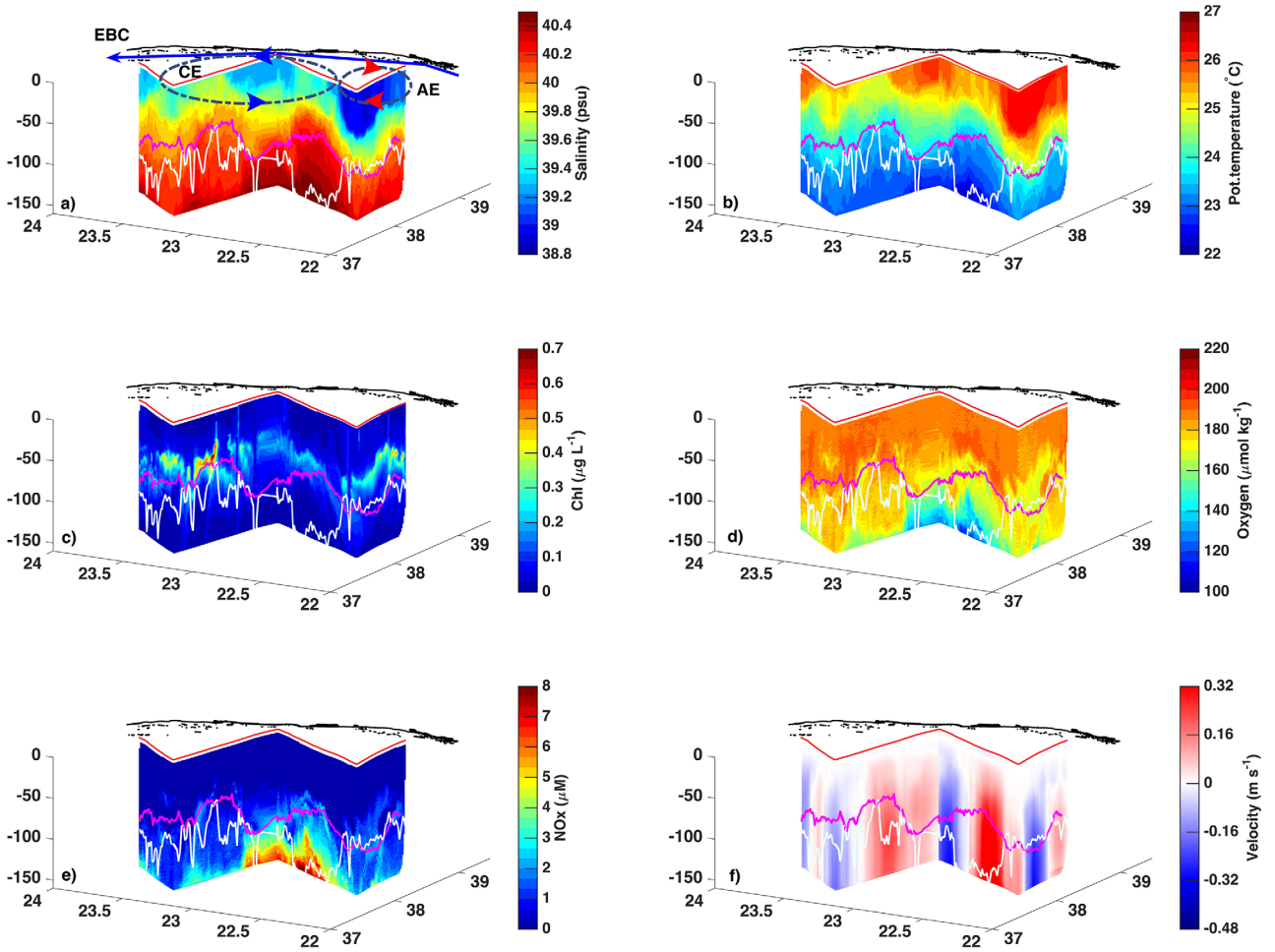

Figure 9. High-resolution ScanFish survey measurements of (a) potential temperature, (b) salinity, (c) chlorophyll (μg L^{-1}), (d) oxygen (μmol kg^{-1}), (e) estimated NOx (μ*M*), and (f) geostrophic velocities (m s^{-1}; level of no motion was set to 150 m) in April 2014. The magenta line represents the mixed layer depth; the grey line illustrates the lower limit of the euphotic depth. The solid red line indicates the surface track of the ScanFish survey within the three-dimensional representation of the data.

is evident in the southern transect and eastern ends of the transects indicated by lower salinity (<39.2) and warmer (>26°C) temperature (Figures 9a and 9b). In the southern transect, the low-salinity water extends to the offshore end of the transect, apparently entrained into the center of the anticyclonic eddy. At the near-coastal points to the north warm, low-salinity water was present, but was not as salty or as warm as along the southern transect. Given the interaction of the two eddies, entrainment of cooler, saltier offshore water

Table 1
Mean and Standard Deviation of the NOx, PO_4^{3-}, N, and CDOM for the Two Cruises*

	Variables	Mean	STD
Both cruises	NOx (N = 169)	5.2 μ*M*	±6.9 μ*M*
	PO_4^{3-} (N = 73)	0.5 μ*M*	±0.3 μ*M*
	N* (N = 73)	−0.1 μ*M*	±2.5 μ*M*
	N* Euphotic (N = 48)	−1.6 μ*M*	±0.3 μ*M*
	N* Aphotic (N = 25)	2.8 μ*M*	±1.5 μ*M*
Fall cruise	NOx:PO_4^{3-} (N = 47)	19.6	±4.8
	CDOM (N = 90)	1.2 ppb	±0.4 ppb
Spring cruise	NOx:PO_4^{3-} (N = 26)	26.3	± 3.7
	CDOM (N = 120)	0.8 ppb	±0.5 ppb

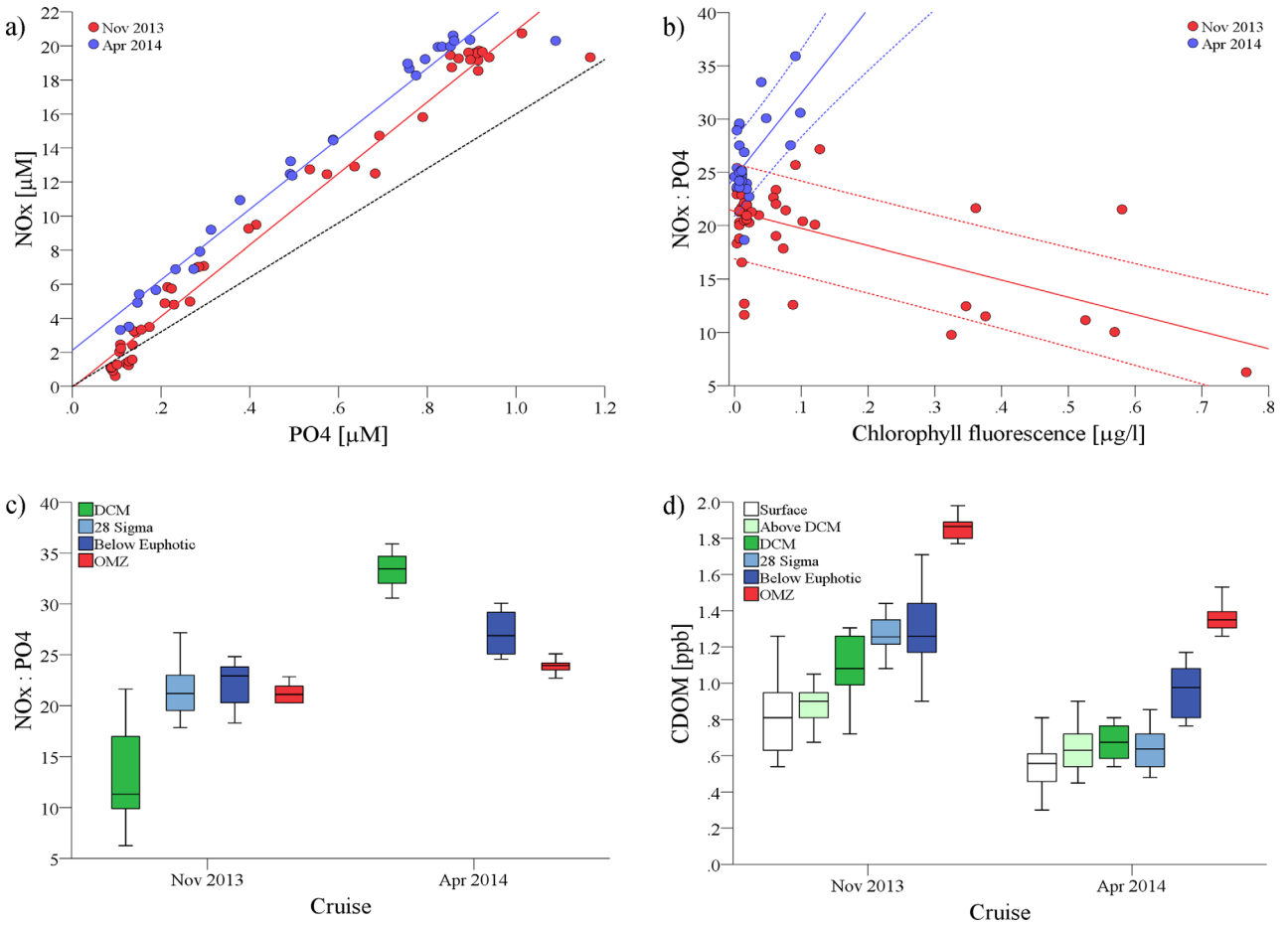

Figure 10. Nutrient inventory and stoichiometric relationships in fall and spring in the central Red Sea. (a) Relationship and linear regressions between nitrogen (NOx) and phosphate (PO_4^{3-}) concentrations (µ*M*) in November 2013 ($R^2 = 0.977$) and April 2014 ($R^2 = 0.970$). The dashed black trend line represents the Redfield ratio. (b) Relationship and linear regressions (±75% confidence intervals) between chlorophyll fluorescence and NOx:PO_4^{3-} in November 2013 ($R^2 = 0.386$) and April 2014 ($R^2 = 0.357$). (c) and (d) Box plots of NOx:PO_4^{3-} and CDOM aggregated by depths layer category (surface = 5 m, above the deep chlorophyll maximum (DCM), DCM, the 28 isopycnal, the bottom of the euphotic zone, OMZ = oxygen minimum layer; boxes = interquartile range, line across the box = median, outer edges = 25th and 75th percentiles, whiskers indicate highest and lowest values).

by the onshore flow between the two eddies may mix with the coastal Gulf of Aden water to increase its salinity (~39.4) and reduce its temperature (~26°C). Zarokanellos et al. (2017) pointed out that eddies may block or redirect the flow of the EBC. In this example, the EBC appears to be entrained by the southern anticyclonic eddy, and is constrained to the coast and mixed with offshore water by the interaction of the eddy pair.

Significant vertical displacement of all the key variables is associated with two eddies (Figures 9a–9e). The depth of the DCM varies by more than 50 m along the course of the ScanFish survey (Figure 9c). The anticyclonic eddy depresses the DCM by about 20–25 m, consistent with the depression of the 26.5 and 27 σ_Θ isopycnals (not shown), between which the DCM is located. Within the cyclonic eddy (transect 2, 3), the chlorophyll maximum was as shallow as about 50 m. Chlorophyll concentrations were very patchy, perhaps driven by stirring associated with the two eddies. Subduction of the chlorophyll was apparent between the two eddies with elevated chlorophyll concentrations extending below 100 m at the offshore end of the southern transect.

The eddy pair plays a key role in the oxygen distribution and may affect productivity in the upper water column. The highest oxygen concentrations in the surface mixed layer (~205 μmol kg^{-1}) coincide with the core of the cyclonic eddy, whereas the lowest surface mixed layer oxygen concentrations (~170 μmol kg^{-1}) occur in the surface mixed layer of the anticyclonic eddy (Figure 9d). Perhaps most importantly, the cyclonic

eddy interacts with EBC, elevates water with low oxygen concentrations (<100 μmol kg^{-1}), and therefore enriched in nutrients (e.g., Naqvi et al., 1986), into the euphotic zone (Figures 9d and 9e). Maximal chlorophyll concentrations are found within the cyclonic eddy, consistent with the probable enhancement of nutrient availability.

3.4. Biogeochemical Modulation Across the Fall and Spring Season

Analysis of the nutrient data provides insight as to how the EBC observed in the fall and the eddy pair observed in the spring affect the vertical and horizontal distribution of nutrients in the CRS. For the full data set, NOx concentrations range from 0.4 μM at the DCM to 20.7 μM at the OMZ, and those of PO_4^{3-} from 0.1 to 1.2 μM (Table 1). NOx and PO_4^{3-} are significantly correlated (Pearson $R = 0.979$, $p < 0.001$). The comparison of the linear fit lines with the superimposed Redfield ratio indicate that phytoplankton in the CRS is generally growing in PO_4^{3-}-deficient water (Figure 10a). The intercepts with the origin indicate that the supply of PO_4^{3-} may limit the growth of primary producers in April due to the overall surplus of NOx relative to PO_4^{3-} (Figure 10a). Conversely in fall both nutrients were supplied in stoichiometric ratios that approached the Redfield ratio. Exact assays of nutrient limitation (bottom-up) and grazing (top-down) control of primary production, however, were beyond the scope of the present study.

Regardless of season, there was a deficit of nitrogen in the CRS, with a significantly different N* value in the euphotic zone and the water below 200 m depths (Table 1; Mann-Whitney U test, $U = 1130.0$, $p < 0.001$). Nutrients were depleted below the limit of detection during both seasons at the surface and in spring also at the $\sigma_\Theta = 28$ isopycnal, and therefore no NOx:PO_4^{3-} could be calculated. Below 200 m, the NOx:PO_4^{3-} ratio ranged from 6.3 to 27.1 in fall and from 18.6 to 35.9 in spring, and were significantly lower in fall than in spring (Mann-Whitney U test, $U = 1122.0$, $p < 0.001$; Table 1, Figure 10b). The described plasticity in NOx:PO_4^{3-} of the present study corroborates that the NOx:PO_4^{3-} ratio is not as uniform as indicated earlier for the Red Sea (NOx:PO_4^{3-} $\approx$ 20–21; cf., Grasshoff, 1969; Naqvi et al., 1986). The survey data also show significantly higher CDOM concentrations in fall relative to the spring (Mann-Whitney U test, $U = 2241.0$, $p < 0.001$; Table 1, Figures 3c and 10c), which may reflect the importance of the transport of nutrient-rich GAIW into the CRS by the EBC. Given that GAIW originates with high concentrations of nutrients and brings elevated chlorophyll into the region, we expect that this contribution will enhance productivity during the summer and fall when GAIW enters the Red Sea.

4. Discussion and Conclusions

The present study uses evidence from remote-sensing, ScanFish surveys, and in situ water sampling to explore physical mechanisms influencing nutrient availability for primary production in the CRS during two seasons (spring and fall). We show how the EBC in fall and the interplay between the eddy pair and EBC in spring alter the physicochemical characteristics of the water masses (i.e., temperature, salinity) and biogeochemical variables (nutrients, chlorophyll, and CDOM), with chlorophyll being a proxy for primary production at the ecosystem scale. The present study corroborates the transport of GASW and GAIW in patches toward the north as observed earlier (Churchill et al., 2014; Sofianos & Johns, 2007; Wafar et al., 2016b). Based on in situ measurements of nutrients, chlorophyll, and CDOM, we show evidence that patches of GAIW may cause higher productivity along their northbound flow path, as indicated by previous observations (Churchill et al., 2014; Wafar et al., 2016b).

The primary mechanism that routes nutrients from the Gulf of Aden to the North is horizontal advection following a thermohaline circulation that resembles an inverse estuary (Grasshoff, 1969). GAIW has usually been characterized by low salinity, low oxygen, and higher nutrients (Churchill et al., 2014), and of which the latter become depleted during the horizontal advection, mixing, and uptake by phytoplankton. It has been proposed that the advection of GAIW toward the north occurs in meandering pattern, and that both wind forcing and eddies play a profound role in altering this transport and subsequent effects of GAIW on planktonic food webs (Bower & Farrar, 2015; Churchill et al., 2014; Kürten et al., 2016; Sofianos & Johns, 2007; Wafar et al., 2016a). The present study shows that the EBC transports lenses of GAIW containing high CDOM and chlorophyll concentrations at intermediate depths from the south through the CRS. The small-scale maxima in chlorophyll and CDOM concentrations observed in the DCM during fall reflect the episodic nature of GAIW transport through the CRS. Elevated chlorophyll and CDOM concentrations, concomitant with lower NOx:PO_4^{3-} ratios indicate the important biogeochemical interplay of the EBC with the primary

production at the end of the stratified summer period in this oligotrophic region of Red Sea. The inverse correlation of NOx:PO_4^{3-} with chlorophyll concentrations may indicate the ecological advantage of rapidly growing diatoms (N:P ≈ 10:1) over cyanobacteria (e.g., *Synechococcus* spp., *Trichodesmium* spp.) that typically attain higher N:P ratios (Deutsch & Weber, 2012; Klausmeier et al., 2004; Weber & Deutsch, 2010).

It has been suggested that eddy-induced upwelling events, with variable position and lifespan, interact with the vertical and horizontal thermohaline circulation by injecting deep-water nutrients into the surface layers (Gaube et al., 2015; Kürten et al., 2016; Martin & Richards, 2001). Elsewhere, it is shown that the interaction of the EBC with mesoscale eddies and may function as a barrier to this northbound thermohaline flow of the EBC, by deflecting the EBC toward the west and offshore (Figure 6, Zarokanellos et al., 2017). Models, remote-sensing of ocean color and altimetry indicate that the CRS is dominated by recurrent and occasionally dipole eddies (Chen et al., 2014; Raitsos et al., 2013; Zhan et al., 2014). We describe a cyclonic/anticyclonic eddy pair as a prominent dynamic feature in spring in our study area. In addition, we examine the interplay of the eddy pair with the EBC that constrains the northward flow against the coast, and entrains GASW into the core of the anticyclonic eddy. This is evidenced by low-salinity, warmer water near the Saudi coast. We show that the eddy pair contributes to the vertical transport of nutrients to the euphotic zone and enhances the primary production.

Our study along with previous studies leaves a number of unanswered questions regarding the impact of mesoscale features on the environment of the Central Red Sea. Future studies of the biogeochemistry of the Red Sea should address the relationships of natural latitudinal gradients with rates of autotrophic carbon fixation (i.e., primary production) and biological nitrogen fixation as a function of new and regenerated production in the Red Sea. Future studies should also elucidate the manner in which eddies affect the variability of these processes in space and time and evaluate implications of such variability for the overall nutrient budget of the Red Sea. The role of the EBC and basin-scale eddies in the supply of nutrients to coral reefs and the exchange of reef-borne nutrients and dissolved organic matter within the dynamic oceanographic catchment of the Red Sea basin (in the sense of, Wyatt et al., 2012) requires investigation. Allochthonous macronutrient subsidies from the open sea may significantly affect biogeochemical processes in adjacent benthic ecosystems and influence ecosystem services and function.

Acknowledgments

Research reported in this publication was supported by the King Abdullah University of Science and Technology (KAUST). Hydrographic data obtained from both cruises can be obtained from Burton H. Jones (KAUST) and Nikolaos D. Zarokanellos (KAUST). The authors gratefully acknowledge the Core Marine Operation Research Lab (CMOR) for their support during the cruises. Special thanks go to Ioannis Georgakakis, Veera B. Yellepeddi, and Mohammedali Nellayaputhenpeedika for their technical support during the cruises. Also, we thank the captain and crew of *R/V Thuwal* for their valued help during the Eddy Shelf Expedition. The SLA was obtained from AVISO and the ocean color products were produced by NASA Ocean Color Group; satellite data are available online through the official websites documented in section 2. We thank Ian Walsh and an anonymous reviewer for their valuable comments and suggestions.

References

Al-Aidaroos, A. M., Karati, K. K., El-Sherbiny, M. M., Devassy, R. P., & Kürten, B. (2017). Latitudinal environmental gradients and diel variability influence abundance and community structure of Chaetognatha in Red Sea coral reefs. *Systematics and Biodiversity*, *15*, 35–48. https://doi.org/10.1080/14772000.2016.1211200

Behrenfeld, M. J., & Kolber, Z. S. (1999). Widespread iron limitation of phytoplankton in the south Pacific Ocean. *Science*, *283*(5403), 840–843. https://doi.org/10.1126/science.283.5403.840

Bethoux, J. P. (1988). Red Sea geochemical budgets and exchanges with the Indian Ocean. *Marine Chemistry*, *24*(1), 83–92. https://doi.org/10.1016/0304-4203(88)90007-2

Bower, A. S., & Farrar, J. T. (2015). Air–sea interaction and horizontal circulation in the Red Sea. In N. M. A. Rasul & I. C. F. Stewart, (Eds.), *The Red Sea, Springer Earth System Sciences* (pp. 329–342). Berlin, Germany: Springer. https://doi.org/10.1007/978-3-662-45201-1_19

Chen, C., Li, R., Pratt, L., Limeburner, R., Beardsley, R. C., Bower, A., . . . Kim, T. (2014). Process modeling studies of physical mechanisms of the formation of an anticyclonic eddy in the central Red Sea. *Journal of Geophysical Research: Oceans*, *119*, 1445–1464. https://doi.org/10.1002/2013JC009351

Churchill, J. H., Bower, A. S., McCorkle, D. C., & Abualnaja, Y. (2014). The transport of nutrient-rich Indian Ocean water through the Red Sea and into coastal reef systems. *Journal of Marine Research*, *72*(3), 165–181. https://doi.org/10.1357/002224014814901994

de Boyer Montégut, C., Madec, G., Fischer, A. S., Lazar, A., & Iudicone, D. (2004). Mixed layer depth over the global ocean: An examination of profile data and a profile-based climatology. *Journal of Geophysical Research*, *109*, C12003. https://doi.org/10.1029/2004JC002378

Deutsch, C., & Weber, T. (2012). Nutrient ratios as a tracer and driver of ocean biogeochemistry. *Annual Review of Marine Science*, *4*, 113–141. https://doi.org/10.1146/annurev-marine-120709-142821

Ducet, N., Le Traon, P. Y., & Reverdin, G. (2000). Global high-resolution mapping of ocean circulation from TOPEX/Poseidon and ERS-1 and −2. *Journal of Geophysical Research*, *105*(C8), 19477–19498. https://doi.org/10.1029/2000JC900063

Edwards, F. J. (1987). Climate and oceanography. In A. J. Edwards & S. M. Head (Eds.), *The Red Sea, A Volume in Key Environment Series* (Chapter 3, pp. 45–69). Oxford, UK: Pergamon Press. https://doi.org/10.1016/B978-0-08-028873-4.50008-6

Ganssen, G., & Kroon, D. (1991). Evidence for red sea surface circulation from oxygen isotopes of modern surface waters and planktonic foraminiferal tests. *Paleoceanography*, *6*(1), 73–82. https://doi.org/10.1029/90PA01976

Gaube, P., Chelton, D. B., Samelson, R. M., Schlax, M. G., & O'Neill, L. W. (2015). Satellite observations of mesoscale eddy-induced Ekman pumping. *Journal of Physical Oceanography*, *45*(1), 104–132. https://doi.org/10.1175/JPO-D-14-0032.1

Gaube, P., McGillicuddy, D. J., Chelton, D. B., Behrenfeld, M. J., & Strutton, P. G. (2014). Regional variations in the influence of mesoscale eddies on near-surface chlorophyll. *Journal of Geophysical Research: Oceans*, *119*, 8195–8220. https://doi.org/10.1002/2014JC010111

Grasshoff, K. (1969). *Zur Chemie des Roten Meeres und des inneren Golfs von Aden nach Beobachtungen von F. S. "Meteor" während der Indischen Ozean Expedition 1964/65* (pp. 1–76). Berlin, Germany: Schweizerbart Science Publishers/Gebrüder Bornträger.

Gruber, N. (2008). *The marine nitrogen cycle: Overview and challenges in nitrogen in the marine environment*. In D. G. Capone, D. A. Bronk, M. R. Mulholland & E. J. Carpenter (Eds.), (2nd Edn., pp.1–50). Cambridge, MA: Academic Press. https://doi.org/10.1016/B978-0-12-372522-6.00001-3

Gruber, N., & Sarmiento, J. L. (1997). Global patterns of marine nitrogen fixation and denitrification. *Global Biogeochemistry Cycles*, *11*(2), 235–266, https://doi.org/10.1029/97GB00077

Halim, Y. (1984). Plankton of the Red Sea and the Arabian Gulf. *Deep Sea Research Part A. Oceanographic Research Papers*, *31*(6–8), 969–982. https://doi.org/10.1016/0198-0149(84)90051-7

Johns, W. E., & Sofianos, S. S. (2012). Atmospherically forced exchange through the Bab el Mandeb Strait. *Journal of Physical Oceanography*, *42*(7), 1143–1157. https://doi.org/.1175/JPO-D-11-0157.1

Kinkade, C. S., Marra, J., Dickey, T. D., Langdon, C., Sigurdson, D. E., & Weller, R. (1999). Diel bio-optical variability observed from moored sensors in the Arabian Sea. *Deep Sea Research Part II: Topical Studies in Oceanography*, *46*, 1813–1831.

Klausmeier, C. A., Litchman, E., Daufresne, T., & Levin, S. A. (2004). Optimal nitrogen-to-phosphorus stoichiometry of phytoplankton. *Nature*, *429*(6988), 171–174. https://doi.org/10.1038/nature02454

Kürten, B., Al-Aidaroos, A. M., Kürten, S., El-Sherbiny, M. M., Devassy, R. P., Struck, U., . . . Sommer, U. (2016). Carbon and nitrogen stable isotope ratios of pelagic zooplankton elucidate ecohydrographic features in the oligotrophic Red Sea. *Progress in Oceanography*, *140*, 69–90. https://doi.org/10.1016/j.pocean.2015.11.003

Kürten, B., Al-Aidaroos, A. M., Struck, U., Khomayis, H. S., Gharbawi, W. Y., & Sommer, U. (2014a). Influence of environmental gradients on C and N stable isotope ratios in coral reef biota of the Red Sea, Saudi Arabia. *Journal of Sea Research*, *85*, 379–394. https://doi.org/10.1016/j.seares.2013.07.008

Kürten, B., Khomayis, H. S., Devassy, R., Audritz, S., Sommer, U., Struck, U., . . . Al-Aidaroos, A. M. (2014b). Ecohydrographic constraints on biodiversity and distribution of phytoplankton and zooplankton in coral reefs of the Red Sea, Saudi Arabia. *Marine Ecology*, *36*(4), 1195–1214. https://doi.org/10.1111/maec.12224

Lee, C. M., Jones, B. H., Brink, K. H., & Fischer, A. S. (2000). The upper-ocean response to monsoonal forcing in the Arabian Sea: Seasonal and spatial variability. *Deep Sea Research Part II: Topical Studies in Oceanography*, *47*(7–8), 1177–1226. https://doi.org/10.1016/S0967-0645(99)00141-1

Maillard, C., & Soliman, G. (1986). Hydrography of the Red Sea and exchanges with the Indian Ocean in summer. *Oceanologica Acta*, *9*(3), 249–269. http://archimer.ifremer.fr/doc/00110/22113/

Martin, A. P., & Richards, K. J. (2001). Mechanisms for vertical nutrient transport within a North Atlantic mesoscale eddy. *Deep Sea Research Part II: Topical Studies in Oceanography*, *48*(4–5), 757–773. https://doi.org/10.1016/S0967-0645(00)00096-5

McGillicuddy, D. J., Robinson, A. R., Siegel, D. A., Jannasch, H. W., Johnson, R., Dickey, T. D., . . . Knap, A. H. (1998). Influence of mesoscale eddies on new production in the Sargasso Sea. *Nature*, *394*(1977), 263–266. https://doi.org/10.1038/28367

Morel, A., & Maritorena, S. (2001). Bio-optical properties of oceanic waters: A reappraisal. *Journal of Geophysical Research*, *106*(C4), 7163–7180. https://doi.org/10.1029/2000JC000319

Murray, S. P., & Johns, W. (1997). Direct observations of seasonal exchange through the Bab el Mandab Strait. *Geophysical Research Letters*, *24*(21), 2557–2560. https://doi.org/10.1029/97GL02741

Naqvi, S. W. A., Hansen, H. P., & Kureishy, T. W. (1986). Nutrient-uptake and regeneration ratios in the red-sea with reference to the nutrient budgets. *Oceanologica Acta*, *9*(3), 271–275. http://drs.nio.org/drs/handle/2264/6222

Özgökmen, T. M., Johns, W. E., Peters, H., & Matt, S. (2003). Turbulent mixing in the Red Sea outflow plume from a high-resolution nonhydrostatic model. *Journal of Physical Oceanography*, *33*(8), 1846–1869. https://doi.org/10.1175/2401.1

Quadfasel, D., & Baudner, H. (1993). Gyre-scale circulation cells in the Red Sea. *Oceanologica Acta*, *16*(3), 221–229. http://archimer.ifremer.fr/doc/00099/21049/

Raitsos, D. E., Pradhan, Y., Brewin, R. J. W., Stenchikov, G., & Hoteit, I. (2013). Remote sensing the phytoplankton seasonal succession of the Red Sea, *PLoS One*, *8*(6), e64909. https://doi.org/10.1371/journal.pone.0064909

Rasul, N. M. A., Stewart, I. C. F., & Nawab, Z. A. (2015). Introduction to the Red Sea: Its origin, structure, and environment. In N. M. A. Rasul & I. C. F. Stewart (Eds.), *The Red Sea*, Springer Earth System Sciences. Berlin, Germany: Springer. https://doi.org/10.1007/978-3-662-45201-1_1

Robitzch, V., Banguera-Hinestroza, E., Sawall, Y., Al-Sofyani, A., & Voolstra, C. R. (2015). Absence of genetic differentiation in the coral *Pocillopora verrucosa* along environmental gradients of the Saudi Arabian Red Sea. *Frontiers in Marine Science*, *2*, 5. https://doi.org/10.3389/fmars.2015.00005

Rodríguez, J., Tintoré, J., Allen, J. T., Blanco, J. M., Gomis, D., Reul, A., . . . Jiménez-Gómez, F. (2001). Mesoscale vertical motion and the size structure of phytoplankton in the ocean. *Nature*, *410*(6826), 360–363. https://doi.org/10.1038/35066560

Sofianos, S. S., & Johns, W. E. (2002). An oceanic general circulation model (OGCM) investigation of the Red Sea circulation, 1. Exchange between the Red Sea and the Indian Ocean. *Journal of Geophysical Research*, *107*(C11), 3196. https://doi.org/10.1029/2001jc001184

Sofianos, S. S., & Johns, W. E. (2003). An oceanic general circulation model (OGCM) investigation of the Red Sea circulation: 2. Three-dimensional circulation in the Red Sea. *Journal of Geophysical Research*, *108*(C3), 3066. https://doi.org/10.1029/2001jc001185

Sofianos, S. S., & Johns, W. E. (2007). Observations of the summer Red Sea circulation. *Journal of Geophysical Research*, *112*, C06025. https://doi.org/10.1029/2006JC003886

Sofianos, S. S., & Johns, W. E. (2015). Water mass formation, overturning circulation, and the exchange of the Red Sea with the adjacent basins. In N. M. A. Rasul & I. C. F. Stewart (Eds.), *The Red Sea, Springer Earth System Sciences*. Berlin, Germany: Springer. https://doi.org/10.1007/978-3-662-45201-1_20

Sofianos, S. S., Johns, W. E., & Murray, S. P. (2002). Heat and freshwater budgets in the Red Sea from direct observations at Bab el Mandeb. *Deep Sea Research Part II: Topical Studies in Oceanography*, *49*(7–8), 1323–1340. https://doi.org/10.1016/S0967-0645(01)00164-3

Souvermezoglou, E., Metzl, N., & Poisson, A. (1989). Red Sea budgets of salinity, nutrients and carbon calculated in the Strait of Bab-El-Mandab during the summer and winter seasons. *Journal of Marine Research*, *47*(2), 441–456. https://doi.org/10.1357/002224089785076244

Wafar, M., Ashraf, M., Manikandan, K. P., Qurban, M. A., & Kattan, Y. (2016a). Propagation of Gulf of Aden intermediate water (GAIW) in the Red Sea during autumn and its importance to biological production. *Journal of Marine Systems*, *154*, 243–251. https://doi.org/10.1016/j.jmarsys.2015.10.016

Wafar, M., Qurban, M. A., Ashraf, M., Manikandan, K. P., Flandez, A. V., & Balala, A. C. (2016b). Patterns of distribution of inorganic nutrients in Red Sea and their implications to primary production. *Journal of Marine Systems*, *156*, 86–98. https://doi.org/10.1016/j.jmarsys.2015.12.003

Weber, T. S., & Deutsch, C. (2010). Ocean nutrient ratios governed by plankton biogeography. *Nature*, *467*(7315), 550–554. https://doi.org/10.1038/nature09403

Wyatt, A. S. J., Falter, J. L., Lowe, R. J., Humphries, S., & Waite, A. M. (2012). Oceanographic forcing of nutrient uptake and release over a fringing coral reef. *Limnology and Oceanography*, *57*(2), 401–419. https://doi.org/10.4319/lo.2012.57.2.0401

Yao, F., Hoteit, I., Pratt, L. J., Bower, A. S., Köhl, A., Gopalakrishnan, G., & Rivas, D. (2014a). Seasonal overturning circulation in the Red Sea: 2. Winter circulation. *Journal of Geophysical Research: Oceans*, *119*, 2263–2289. https://doi.org/10.1002/2013JC009331

Yao, F., Hoteit, I., Pratt, L. J., Bower, A. S., Zhai, P., Köhl, A., & Gopalakrishnan, G. (2014b). Seasonal overturning circulation in the Red Sea: 1. Model validation and summer circulation. *Journal of Geophysical Research: Oceans*, *119*, 2238–2262. https://doi.org/10.1002/2013JC009004

Zarokanellos, N. D., Papadopoulos, V. P., Sofianos, S. S., & Jones, B. H. (2017). Physical and biological characteristics of the winter-summer transition in the Central Red Sea. *Journal of Geophysical Research: Oceans*, *122*, 6355–6370. https://doi.org/10.1002/2017JC012882

Zhai, P., Pratt, L. J., & Bower, A. (2015). On the crossover of boundary currents in an idealized model of the Red Sea. *Journal of Physical Oceanography*, *45*(5), 1410–1425. https://doi.org/10.1175/JPO-D-14-0192.1

Zhan, P., Subramanian, A. C., Yao, F., & Hoteit, I. (2014). Eddies in the Red Sea: A statistical and dynamical study. *Journal of Geophysical Research: Oceans*, *119*, 3909–3925. https://doi.org/10.1002/2013JC009563